Title

A LEED CRYSTALLOGRAPHY STUDY OF THE (2x2)-C2H3 STRUCTURE OBTAINED AFTER ETHYLENE ADSORPTION ON Rh(111)

Authors

Koestner, R.J.
Hove, M.A. Van
Somorjai, G.A.

Publication Date

1982-06-01

LBL-13598
Preprint

Lawrence Berkeley Laboratory
UNIVERSITY OF CALIFORNIA

Materials & Molecular
Research Division

Submitted to Surface Science

A LEED CRYSTALLOGRAPHY STUDY OF THE (2x2)-C_2H_3 STRUCTURE OBTAINED AFTER ETHYLENE ADSORPTION ON Rh(111)

R.J. Koestner, M.A. Van Hove and G.A. Somorjai

June 1982

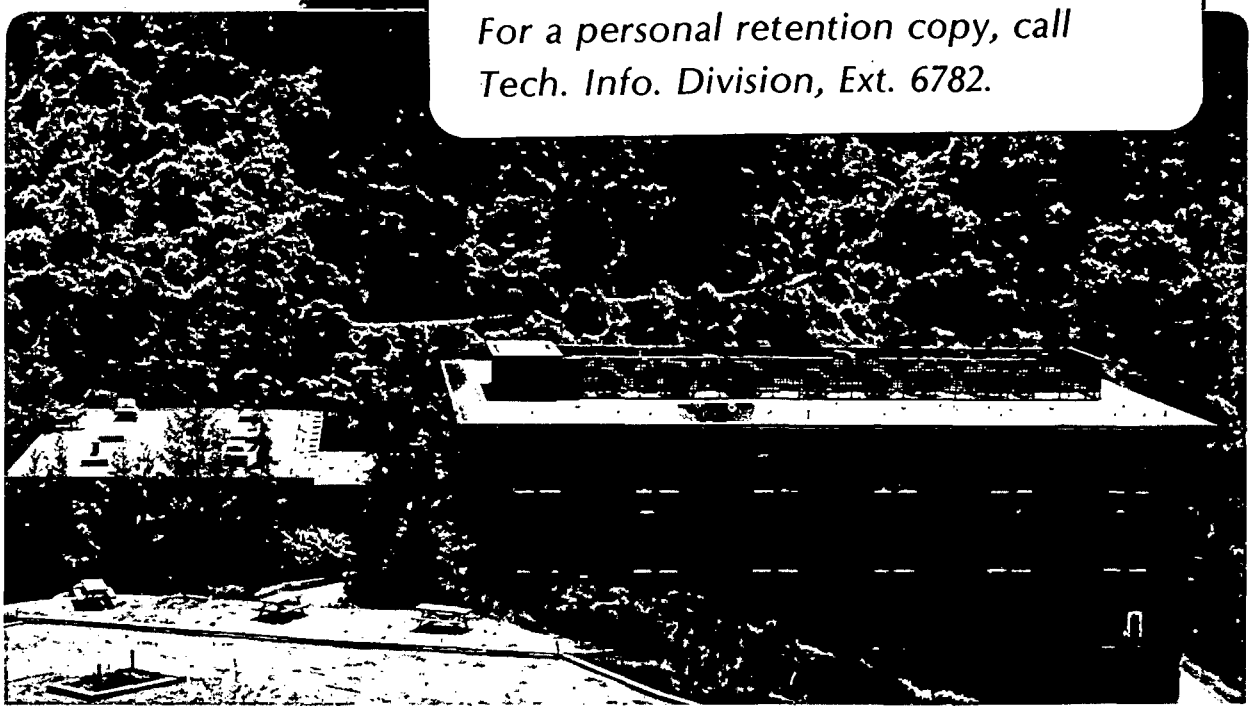

Prepared for the U.S. Department of Energy under Contract DE-AC03-76SF00098

DISCLAIMER

LBL-13598

A LEED CRYSTALLOGRAPHY STUDY OF THE (2x2)-C_2H_3 STRUCTURE OBTAINED AFTER ETHYLENE ADSORPTION ON Rh(111)

R. J. Koestner, M. A. Van Hove and G. A. Somorjai

Materials and Molecular Research Division, Lawrence Berkeley Laboratory,

and

Department of Chemistry, University of California

Berkeley, CA 94720

ABSTRACT

The structure of the Rh(111)-(2x2)-C_2H_3 overlayer that was obtained upon the adsorption of ethylene has been determined using a LEED intensity analysis. In agreement with a prior HREELS study, an ethylidyne ($\equiv CCH_3$) species is found to stand perpendicularly above an hcp hollow site with a carbon-carbon distance of 1.45 ± 0.10Å and a metal-carbon distance of 2.03 ± 0.07Å. The Zanazzi-Jona and Pendry R-factors for this structure are 0.49 and 0.52, respectively. By comparison with similar organometallic complexes, the relatively short carbon-carbon distance and long metal-carbon distance can be explained by $\sigma - \pi$ hyperconjugation of the surface thylidyne fragment.

This work was supported by the Director, Office of Energy Research, Office of Basic Energy Sciences, Materials Science Division of the U.S. Department of Energy under contract DE-AC03-76SF00098.

1. Introduction

The structure of ethylene adsorbed on the Pt(111) surface has been intensively investigated[1-7] in the last few years and a progression of different surface phases is believed to form with increasing temperature. At 270-500K, the ethylene overlayer was found to partially dehydrogenate and form a (2x2) lattice of ethylidyne ($\equiv C-CH_3$) with a one-quarter monolayer coverage. Although this Low Energy Electron Diffraction (LEED) result[8] was somewhat controversial at first, it has now been supported by High Resolution Electron Energy Loss Spectroscopy (HREELS)[9,10] and Angle-Resolved Ultraviolet Photoelectron Spectroscopy (ARUPS).[11]

Interestingly, Rh(111)[12], Pd(111)[13], and Pt(100)[14] have ethylene overlayers with HREEL spectra nearly identical to those of the ethylidyne structure on Pt(111), indicating that the same species forms on these surfaces. The vibrational study on the Rh(111) surface showed that two different ethylidyne phases form as a function of temperature. Between 230 and 270 K a (2x2) lattice of ethylidyne appears at a one-quarter monolayer coverage, while heating to 270-420 K produces a c(4x2) lattice of ethylidyne with the same coverage. Above 420 K, the carbon-carbon bond breaks leaving a C-H species present on the surface to 700 K.

In this paper, we shall present a structural determination of the Rh(111)-(2x2)-C_2H_3 phase using a LEED intensity analysis. Our study confirms the ethylidyne model found by HREELS. Although LEED is not sensitive to the hydrogen positions, the carbon-carbon and metal-carbon distances that we find are most consistent with the ethylidyne model. Besides confirming the HREELS result, our study provides additional bonding information on the ethylidyne species. First, ethylidyne is clearly shown to stand above an hcp hollow site rather than the fcc hollow found for ethylidyne on Pt(111). This change in

adsorption site could be caused by the presence of coadsorbed hydrogen on Rh(111). Second, the measured carbon-carbon (1.45Å) and metal-carbon (2.03Å) bond distances for ethylidyne on Rh(111) can be explained by σ-π hyperconjugation. That is, the lower (or apical) carbon atom in ethylidyne is probably carbynic (sp-hybridized) permitting effective delocalization of the C-H group's σ-bond electrons into the metal valence band. The ethylidyne bonding to the surface can be imagined as a non-directional triple bond rather than three separate sp^3 orbitals pointed toward different Rh atoms. Substantial evidence for this unusual bonding arrangement is also present in similar organometallic clusters, such as $Co_3(CO)_9CCH_3$.

2. Experimental

The rhodium crystal of >99.9% purity was cut to within 1/2° of the (111) plane and mechanically polished with a sequence of alumina emery papers and ~ 1 μ diamond paste. The crystal was mounted on rhodium foil that in turn was attached to a Varian manipulator; the "flip" mechanism available was modified to allow an azimuthal rotation of about 90°. Before the manipulator was inserted into the UHV chamber, the crystal surface normal and the azimuthal rotation axis were made parallel to within 1/2° by laser reflection. The vacuum system is equipped with four-grid LEED/Auger optics, glancing incidence Auger electron gun, and a quadrupole mass spectrometer head; the base pressure remained at 5×10^{-10} - 1×10^{-9} torr during the experiments with the major background gas constituents being H_2 and CO.

An Auger electron spectrum[15] of the crystal after only a few cleaning cycles showed substantial sulfur and boron as well as smaller chlorine and carbon peaks. Boron (a 17 ppm bulk impurity) proved most troublesome to remove; extended Ar^+ bombardments (1-3μamps, 1.2kV), that were frequently

interrupted with five minute annealing at 800°C or O_2 treatments (flowing $5x10^{-7}$ torr O_2 at 700°C), were needed to largely deplete the near surface region of boron. The sulfur and boron peak heights were then reduced to small values[15] that remained constant even after many additional cleaning cycles. The residual, probably subsurface, oxygen seen by Thiel et al.[16] after O_2 treatments is just below the detection limit of our retarded field Auger spectra[15]; but our Rh(111)-(2x2)-C_2H_3 diffraction beam intensity spectra did not change when oxygen treatments were used for sample cleaning rather than Ar^+ bombardments.

Before ethylene exposures, the crystal was routinely flashed to 400°C to remove pre-adsorbed carbon monoxide and hydrogen; the crystal would then cool to -30°C in less than ten minutes. However, carbon monoxide would be displaced from the chamber walls during the ethylene exposure and would then coadsorb to give approximately a .05 monolayer coverage, as determined by thermal desorption yield experiments.

After an ordered ethylene overlayer was obtained, the intensity vs. voltage (I-V) curves for the various diffraction beams were collected using a photographic method, similar to that already described.[17] A Beattie Varitron view camera (fitted with a Bencher external shutter and an 85 mm, f1.8 Nikon lens) was adjusted for the maximum aperture and a 1/2 sec exposure time to photograph the LEED pattern displayed on a fluorescent screen; a high speed Kodak film (panchromatic 2484) was also used. The photographs of the LEED spot pattern, taken at 2eV intervals, were digitized with a scanning microdensitometer; the resulting density map at successive energies was converted with a new computer program into the desired I-V profiles. The resulting I-V curves were checked for a three-fold symmetry at normal incidence ($\theta=0°$) and a remaining mirror-plane symmetry off normal incidence ($\theta\neq0$, $\phi=0°$); in addition,

each I-V profile was reproduced in a second, independent experiment. For use in the reliability-factor analysis, the I-V spectra were then averaged over degenerate beams and independent runs, normalized to a 1μamp incident beam current, and smoothed twice with a three-point formula. The entire set of 48 independent intensity curves that were collected at 4 different angles of incidence (θ=0°; θ=11°, ϕ=0°; θ=21°, ϕ=0°; and θ=31°, ϕ=0°) the (2x2)-C_2H_3 structure determination are available on request in either a digitized or plotted form.

Similar to our finding in an earlier study[15] of the Rh(111)-($\sqrt{3}$ x $\sqrt{3}$)R30°-CO, the incident LEED beam would first slightly improve the ordering of the overlayer structure, then an exponential decay with electron exposure would begin in the fractional-order diffraction spot intensities. Figure 1 shows the change in the (0,1/2) beam intensity for the (2x2)-C_2H_3 overlayer as a function of electron beam exposure; there is a slight increase in the beam intensity during the first 15μamp-sec and then an exponential decay that reaches half-maximum intensity in ~36μamp-sec. The extent of enhanced ordering by the electron beam depended on the amount of coadsorbed background hydrogen on the surface; as the coadsorbed hydrogen coverage increased, a longer electron beam exposure was necessary to reach the maximum spot intensity. In yet another similarity with the earlier CO/Rh(111) study,[15] a semi-log plot of the (0,1/2) beam intensity vs. electron exposure (see Figure 2) for the (2x2)-C_2H_3 phase again shows two rather different decay constants. Although the initial decay rate for the ethylene overlayer (α_1 = .029μamp-sec^{-1}) is about twice as fast as for the carbon monoxide overlayer (α_1 = .016μamp-sec^{-1}), the second decay rates are essentially identical (α_2 = .0086μamp-sec^{-1} for ethylene, α_2 = .0088μamp-sec^{-1} for carbon monoxide).

In light of this sensitivity, the electron beam damage was minimized by

moving the beam across the crystal during photography,[18] thus limiting the electron beam exposure of any given region of the surface to less than 25μamp-sec. As a result, the LEED spots associated with the ethylene overlayer would stay within 5-10% of their maximum intensity during photography.

3. LEED Theory

The LEED calculations for the Rh(111)-(2x2)-C_2H_3 structure were performed with convergent multiple scattering through renormalized forward scattering.[19] The rhodium atoms are represented by a band structure muffin-tin potential,[20] used in previous LEED calculations for rhodium surfaces.[15,21] For the adsorbed molecular species we used the approach indicated by Kesmodel et al.[8,22] for a similar molecular species on Pt(111). The hydrogen atoms are ignored, being weak electron scatterers. The spherically symmetrical potential inside the carbon muffin-tin spheres was obtained[22.a] from molecular-orbital wave functions given by Palke and Lipscomb[23] in a self-consistent field treatment for acetylene. The potential consists of an electrostatic term and a Slater exchange term, and some overlap with nearby platinum atoms is included. An imaginary part of the potential proportional to $E^{1/3}$ was chosen. Rhodium thermal vibration amplitudes were increased by a factor of 1.4 relative to the bulk value for Rh, while the adatoms were given double the bulk vibration amplitudes.

Theory and experiment are compared through a set of R-factors (reliability factors) and their average. One R-factor measures the fraction of the energy range with slopes of opposite signs in the experimental and theoretical I-V curves, two R-factors are based on the intensity differences (both in absolute value and squared), and the others are the Zanazzi-Jona and Pendry R-factors (they are called ROS, R1, R2, RRZJ and RPE, respectively, in Refs. 15

and 21f). We not only average R-factors over all available beams but also contrast the R-factors for different beams, looking for coincidence in the structural predictions by the different beams.

4. Results and Discussion

i) (2x2) → c(4x2) Transition

To produce the (2x2)-C_2H_3 structure, the crystal temperature was held at 220-270K while the ethylene gas (Matheson Gas Products, 99.5% pure) was introduced with aneedle doser for an uncorreted exposure of 0.5L. An over- or under-exposure of ethylene would cause the ethylene layer to disorder. Upon heating the crystal gently to room temperature over the course of several hours, the LEED pattern indicated that the overlayer first disordered and then reordered into a c(4x2) structure. The diffraction patterns for the (2x2) and c(4x2) overlayers are shown in Fig. 3. If sufficient coadsorbed atomic hydrogen is present on the Rh(111) surface, both (2x2) and c(4x2) structures can form simultaneously at 230K. The c(4x2) structure is thought to consist of the same species as the (2x2) structure, based on HREELS results. However a LEED analysis has so far not been able to confirm this.

ii) Determiantion of the (2x2) Ethylene Overlayer Structure

Four different adsorption sites were tested for the Rh(111)-(2x2)-C_2H_3

determination; they are the atop (aaABC...), the hcp hollow (bbABC..., xbABC..., and bABC...), the fcc hollow (ccABC...), and the bridge (ddABC...) sites. (The notation aaABC..., etc. indicates lateral layer positioning as in the ABCABC... stacking arrangement of bulk fcc lattices; lower-case letters refer to carbon atoms, d designating a bridged location and x a general location.) The two hollow sites are distinguished by the presence (hcp) or absence (fcc) of second layer atoms directly beneath them. At each site, the carbon-carbon axis was kept perpendicular to the surface except for the hcp hollow (xbABC...) where the axis was tilted 28-42° from the normal along the [0$\bar{1}$1] direction; the carbon-carbon and carbon-metal distances were then varied in 0.1Å increments. Table I summarizes the set of all 220 structural models tried.

The comparison between theoretical and experimental I-V curves at normal incidence (nine independent beams) eliminated the atop (aaABC...) and fcc hollow (ccABC...) sites as well as the models with a tilted carbon-carbon axis (xbABC...) and with a quarter monolayer of atomic carbon (bABC...). Figure 4 shows the average R-factor contour plots for the remaining hcp hollow (bbABC...) and bridge (ddABC...) sites. We see that the minimum R-factor reached in both plots, when varying the metal-carbon and carbon-carbon distances, is about the same (0.29 for the hcp hollow, 0.30 for the bridge). Yet the contours for the hcp hollow site are much steeper than those for the bridge site.

To confidently distinguish between these two models, we moved to the intensity curves (thirty-nine independent beams) taken at three off-normal incidence angles. Figure 5 shows the R-factor contour plots for the hcp hollow and bridge sites at each of the three off-normal incidence angles. The R-factor minima for the hcp hollow site are significantly lower than those for

the bridge site at θ=21° and θ=31°, while we again notice that the contours are much steeper for the hcp hollow than for the bridge site. The importance of off-normal incidence intensity curves to help distinguish between two closely competing structural models has already been observed in the LEED determination of Pt(111)-(2x2)-C_2H_3.[8] Also, the metal-carbon and carbon-carbon distances are much more consistent for the hcp hollow site at the different polar angles.

The R-factor contours obtained in this determination are comparable both in shape and magnitude to those available in two other molecular structure determinations with dynamical LEED. For the Rh(111)-($\sqrt{3}$ x $\sqrt{3}$)R30°-CO system,[15] a Zanazzi-Jona reliability factor of 0.40 and a Pendry factor of 0.50 were obtained, while Pendry R-factors of 0.50 and 0.40 were found for CO on Ni and Cu (100),[24] respectively. We find a Zanazzi-Jona R-factor of 0.49 and a Pendry R-factor of 0.52 for the Rh(111)-(2x2)-C_2H_3 determination. It is interesting that the R-factor contour plots around the minimum have, in the present work as well as in the CO investigations, an elongated elliptical shape with a major-to-minor axis ratio of up to ~4:1. This elongation, which becomes less pronounced at polar angles further off normal incidence, implies a greater uncertainty in the position of the underlying carbon atom than the overlying oxygen (for the CO work) or carbon atom (for this study). This feature has already been discussed in Refs. 15 and 24.

Our analysis gives the projected metal-carbon ($d_{\perp RhC}$) and carbon-carbon ($d_{\perp CC}$) distances to be 1.31 ± 0.1 Å and 1.45 ± 0.1 Å, respectively; these values represent weighted averages over the polar-angle data that account for the different number of beam profiles at each angle. The individual metal-carbon ($d_{\perp RhC}$) and carbon-carbon ($d_{\perp CC}$) distances for each angle can be found in the R-factor plots (Figs. 4 and 5). An ethylidyne species (≡C-CH_3) is

strongly implied by these bond distances in agreement with earlier HREELS work.

iii) Comparison of Ethylidyne Adsorbed on the Pt(111) and Rh(111) Surfaces:

The LEED determination of the Pt(111)-(2x2)-C_2H_3 structure showed that ethylidyne stands above an fcc hollow site, while our study clearly indicates that ethylidyne stands above an hcp hollow site on the Rh(111) surface. A possible explanation why ethylidyne would select different adsorption sites on the Pt and Rh surfaces involves the role of coadsorbed hydrogen. Thermal Desorption Spectra (TDS) of the Rh[12] and Pt(111)-(2x2)-C_2H_3[25] overlayers show that the extra hydrogen released to form ethylidyne from ethylene remains on the Rh surface (<270K) but desorbs from Pt(300K). Since hydrogen has been observed to dissociate and sit above a hollow site on the Ni(111)[26] and Pt(111)[27] surfaces, it is possible that the coadsorbed hydrogen on the Rh(111) surface may occupy a fcc hollow site and thereby block this site for ethylidyne adsorption. This argument suggests that ethylidyne may choose a fcc hollow site in the c(4x2) lattice that forms at room temperature. However, it should be realized that the adsorbed ethylene has only a quarter-monolayer coverage so there are still other fcc hollow sites present on the surface for ethylidyne to occupy at 230K if it were sufficiently mobile.

In Table II, we list the bond lengths for ethylidyne on Rh and Pt(111). We notice that the carbon-carbon distance is longer and the carbon covalent radius shorter for Pt than Rh. These differences may be explained by the different hollow sites that ethylidyne occupies on Rh and Pt, as we will see in the next section.

5. Comparison with Organometallic Clusters: Evidence for σ-π Hyperconjugation

The objective of our structural studies is to gain more information on the bonding of the molecule or complex being investigated; in this section, we shall interpret our structural results in the context of similar organometallic compounds that have been extensively studied to date. The carbon-carbon bond distance (1.45Å) for the Rh(111)-(2x2)-C_2H_3 structure is smaller than the single bond distances (1.53-1.54Å) found in saturated hydrocarbons and substantially larger than the double (1.34Å) or triple (1.20Å) bond lengths found in unsaturated hydrocarbons. Although Figure 5 shows some scatter in the measured carbon-carbon distance in ethylidyne at different polar angles, the range is well below that expected for a single bond (1.54-1.53Å).

An attractive explanation for the slight double-bond character in the carbon-carbon distance of ethylidyne is σ-π hyperconjugation. We can write two resonance structures (I,II) for the surface ethylidyne species. This

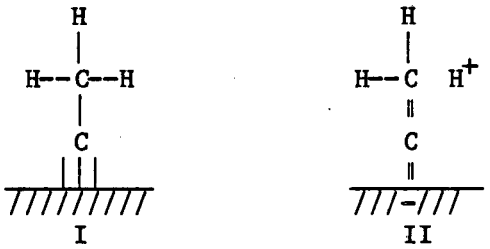

resonance permits the energetically favorable delocalization of electrons from the C-H bond into the metal valence band, but requires that the lower (apical) carbon be sp-hybridized. The lower carbon atom then bonds to the surface in a delocalized fashion much like that in metallocene clusters; this bond though is fairly weak because of the poor overlap between the carbon p and the metal d orbitals.

Table III lists the carbon-carbon bond distances for a group of organic,

organometallic, and surface species. The single bonds in these species acquire some double-bond character due to resonance. For diacetylene, the carbon-carbon single bond is shortened to 1.37Å from delocalization of the π-electrons, while for propylene, the carbon-carbon single bond is shortened to 1.51Å due to σ-π hyperconjugation. We notice that the apical carbon in ethylidyne appears to be sp^2-hybridized in $(CO)_9Co_3C-CH_3$ but sp-hybridized in Rh(111)-(2x2)-CCH_3. This is to be expected since the metal valence band can better delocalize the C-H σ-bond electrons than the trinuclear cluster can and thus can better afford to pay for the energetically costly sp-hybridization of the lower carbon atom.

If the carbon-carbon distance in surface ethylidyne is shorter than that in the corresponding clusters, we expect the carbon-metal distance in surface ethylidyne to be longer than its organometallic counterpart. Table IV indeed shows the covalent radius of the apical carbon in surface ethylidyne to be about 0.69Å and in the clusters to be about 0.66Å; these values are very consistent for all the organometallic compounds listed on the one hand and for the different polar-angle measurements of the surface species on the other. Thus, the structural evidence for the organometallic compounds, $M_3(CO)_9$ CCH_3, and the Rh(111)-(2x2)-C_2H_3 overlayer indicates a sp-hybridized apical carbon and significant σ-π hyperconjugation in the surface ethylidyne group. Table V summarizes the complementary electronic evidence available on the organometallic cluster, $Co_3(CO)_9CCH_3$, for ~ sp^2-hybridization and σ-π hyperconjugation.

Let us now consider the bond lengths for ethylidyne on the Pt(111) surface that are listed in Table II. The larger carbon-carbon distance and much shorter carbon covalent radius found on the Pt surface may arise because no R-factor analysis was used to interpolate between the tested bond distances. Yet another explanation can account for the different bond lengths of ethyli-

dyne on Rh and Pt. On Pt, the ethylidyne stands above a fcc rather than hcp hollow site; this could pull the apical carbon of ethylidyne into the hollow site and increase the sp-d_z2 overlap with the third layer Pt atom. In turn, the apical carbon's sp^3-orbital overlap with the d_{xz}, d_{yz} metal orbitals would strengthen and thereby reduce the chance for sp-rehybridization and σ-π hyperconjugation.

6. Summary

Ethylidyne is found to form on the Rh(111) surface between 230 and 270 K; it orders into a (2x2) lattice with one molecule per unit cell. The CCH_3 fragment stands perpendicularly above an hcp hollow site rather than the fcc hollow site found for ethylidyne on Pt(111). This change in adsorption sites for Pt and Rh may be due to the coadsorbed hydrogen present only on the Rh surface; this hydrogen could occupy a fcc hollow site that could block ethylidyne adsorption if the CCH_3 group is not very mobile.

The carbon-carbon (1.45 Å) and metal-carbon (2.03 Å) distances determined in this study produce a Pendry R-factor of 0.52 and a Zanazzi-Jona R-factor of 0.49. The distances suggest that the carbon atom bound to the surface is carbynic (sp-hybridized) and that the C-H bond electron density is delocalized into the metal valence band.

Acknowledgement

We gratefully acknowledge the technical assistance of Greg Lewis during the course of this work. This work was supported by the Director, Office of Energy Research, Office of Basic Energy Sciences, Materials Science Division of the U.S. Department of Energy under contract DE-AC03-76SF00098.

References

1) H. Ibach, H. Hopster and B. Sexton, Applied Phys. 14, 21 (1977).

2) H. Ibach and S. Lehwald, J. Vac. Sci. Tech. 15, 407 (1978).

3) T. E. Felter and W. H. Weinberg, Surf. Sci. 103, 265 (1981).

4) J. E. Demuth, Surf. Sci. 84, 315 (1979).

5) L. L. Kesmodel, R. C. Baetzold and G. A. Somorjai, Surf. Sci. 66, 299 (1977).

6) P. C. Stair and G. A. Somorjai, JCP 66, 2036 (1977).

7) W. J. Lo, Y. W. Chung, L. L. Kesmodel, P. C. Stair and G. A. Somorjai, Solid State Comm. 22, 335 (1977).

8) L. L. Kesmodel, L. H. Dubois and G. A. Somorjai, JCP 70, 2180 (1979).

9) H. Ibach (to be published).

10) S. F. A. Kettle, I. A. Oxton, D. B. Powell, N. Sheppard and P. Skinner, J. Chem. Soc. Faraday Trans. 77, 397 (1981).

11) M. R. Albert, L. G. Sneddon, E. W. Plummer and T. Gustafsson, ACS Annual Meeting, N.Y., N.Y. (1981); submitted to Surface Science.

12) L. H. Dubois, D. G. Castner and G. A. Somorjai, JCP 72, 5234 (1980).

13) L. L. Kesmodel and J. A. Gates, submitted to Surf. Sci. Lett.

14) H. Ibach, Proceedings Conference on Vibrations in Adsorbed Layers (Jülich, Germany, 1978).

15) R. J. Koestner, M. A. Van Hove and G. A. Somorjai, Surf. Sci. 107, 439 (1981).

16) P. A. Thiel, J. T. Yates, Jr. and W. H. Weinberg, Surf. Sci. 82, 22 (1979).

17) P. C. Stair, T. J. Kaminska, L. L. Kesmodel and G. A. Somorjai, Phys. Rev. B11, 623 (1975).

18) M. Passler, A. Ignatiev, F. Jona, D. W. Jepsen and P. M. Marcus, Phys.

Rev. Lett. 43, 360 (1979).

19) a. J. B. Pendry, "Low Energy Electron Diffraction", Academic Press, London (1974). b. M. A. Van Hove and S. Y. Tong, "Surface Crystallography by LEED", Springer, Heidelberg (1979).

20) V. L. Moruzzi, A. R. Williams and J. F. Janak, "Calculated Electronic Properties of Metals", Pergamon, New York (1978).

21) a. D. C. Frost, K. A. R. Mitchell, F. R. Shepherd and P. R. Watson, Proc. 7th IVC and 3rd ICSS, Vienna (1977), p. 2725. b. K. A. R. Mitchell, F. R. Shepherd, P. R. Watson, and D. C. Frost, Surf. Sci. 64, 737 (1977). c. P. R. Watson, F. R. Shepherd, D. C. Frost and K. A. R. Mitchell, Surf. Sci. 72, 562 (1978). d. C.-M. Chan, P. A. Thiel, J. T. Yates, Jr. and W. H. Weinberg, Surf. Sci. 76, 296 (1978). e. F. R. Shepherd, P. R. Watson, D. C. Frost and K. A. R. Mitchell, J. Phys. C11, 4591 (1978). f. M. A. Van Hove and R. J. Koestner, Proc. Conf. on Determination of Surface Structure by LEED, Plenum, New York (1981).

22) a. L. L. Kesmodel, R. C. Baetzold and G. A. Somorjai, Suf. Sci. 66, 299 (1977). b. L. L. Kesmodel, L. H. Dubois and G. A. Somorjai, Chem. Phys. Lett. 56, 267 (1978).

23) W. E. Palke and W. N. Lipscomb, J. Am. Chem. Soc. 88, 2384 (1966).

24) a. S. Andersson and J. B. Pendry, Phys. Rev. Lett. 43, 363 (1979). b. S. Andersson and J. B. Pendry, J. Phys. C. (in press).

25) M. Salmerón and G. A. Somorjai, J. Phys. Chem. (in press).

26) W. Ho, J. DiNardo and E. W. Plummer, J. Vac. Sci. Tech. 17, 134 (1980).

27) A. M. Baró, H. Ibach and H. D. Bruchmann, Surf. Sci. 88, 384 (1979).

28) Tables of Interatomic Distances and Configurations in Molecules and Ions, L. E. Sutton, ed., Chemical Society Special Publication, Vols. 11, 18.

29) M. D. Brice and B. R. Penfold, Inorg. Chem. 11, 1381 (1972).

30) R. J. Dellaca, B. R. Penfold, B. H. Robinson, W. T. Robinson and J. L. Spencer, Inorg. Chem. 9, 2204 (1970).

31) R. J. Dellaca and B. R. Penfold, Inorg. Chem. 10, 1269 (1971).

32) P. W. Sutton and L. F. Dahl, JACS 89, 261 (1967).

33) G. M. Sheldrick and J. P. Yesinowski, J. Chem. Soc. Dalton, p. 873 (1975).

34) J. P. Yesinowski and D. Bailey, J. Organometallic Chem. 65, 627 (1974).

35) M. D. Brice, B. R. Penfold, W. T. Robinson and S. R. Taylor, Inorg. Chem. 9, 362 (1970).

36) M. D. Brice, R. J. Dellaca, B. R. Penfold and J. L. Spencer, Chem. Commun. p. 72 (1971).

37) G. Pályi, F. Piacenti and L. Markó, Inorg. Chim. Acta Rev. p. 109 (1970).

38) F. Klanberg, W. B. Askew and L. J. Guggenberger, Inorg. Chem. 7, 2265 (1968).

39) V. Bätzel, V. Müller and R. Allmann, J. Organomet. Chem. 102, 109 (1975).

40) M. D. Brice, B. R. Penfold, W. T. Robinson and S. R. Taylor, Inorg. Chem. 9, 362 (1970).

41) D. Seyferth, Adv. Organomet. Chem. 14, 97 (1976).

42) D. C. Miller and T. B. Brill, Inorg. Chem. 17, 240 (1978).

Table Captions

I) Summary of the 220 different structural models tested in the LEED determination of Rh(111)-(2x2)-C_2H_3.

II) Comparison of ethylidyne bond distances on Pt(111) and Rh(111).

III) Variation of carbon-carbon bond lengths for organometallic clusters and surface species: evidence for sp and sp^2 hybridization of the apical carbon for $YCCo_3(CO)_9$.

IV) Comparison of apical carbon covalent radii for alkylidyne clusters and ethylidyne on Rh(111).

V) Complementary electronic evidence for sp or sp^2 rehybridization and hyperconjugation in $Co_3(CO)_9CCH_3$.

Figure Captions

1) Plot of (0 1/2) beam intensity vs. electron beam exposure.

2) Semilog plot of (0 1/2) beam intensity vs. electron beam exposure.

3) LEED patterns from surface structures produced by C_2H_4 adsorption on Rh(111). (a) clean Rh(111) at 93eV, (b) (2x2)-C_2H_3 at 74eV, and (c) c(4x2)-C_2H_3 at 68eV.

4) R-factor contour plot for bridge and hollow sites at $\theta = 0°$. (Contour levels occur at 0.025 intervals.)

5) R-factor contour plot for bridge and hollow sites at $\theta = 0°$. (Contour levels occur at 0.025 intervals.)

6) Real spare structures for the Rh(111)-(2x2)-C_2H_3 overlayer (lower panel) and the Rh(111)-c(4x2)-C_2H_3 overlayer (upper panel).

Table I

Summary of the 220 different structural models tested in the LEED determination of Rh(111)-(2x2)-C_2H_3.

Site	$d_{\perp RhC}$[Å]	$d_{\perp CC}$[Å]	$d_{\parallel CC}$[Å]	Remarks
ccABC...	1.1(.1)1.4	1.1(.1)1.6	0	
bbABC...	1.1(.1)1.8	1.1(.1)1.6	0	
xbABC...	1.1(.1)1.4	1.1(.1)1.6	.74	gives tilt angle θ_{CC}=42.3, 30, 27.5° at $d_{\perp CC}$=1.1, 1.5, 1.6Å, respectively
aaABC...	1.1(.1)2.2	1.1(.1)1.6	0	
ddABC...	1.1(.1)1.8	1.1(.1)1.6	0	
bABC...	1.1(.1)1.4	-	-	no 2nd C; 1/4 monolayer C coverage

Table II

Comparison of Ethylidyne Bond Distances on Pt(111) and Rh(111). (c = carbon-carbon distance, m = metal-carbon distance, r_M = measured metallic radius, r_C = carbon covalent radius).

	c(Å)	m(Å)	r_M(Å)	r_C(Å)=m-r_M
Rh(111)-(2x2)-C_2H_3	1.45	2.03	1.34	0.69
Pt(111)-(2x2)-C_2H_3	1.50	2.00	1.39	0.61

Table III

Variation of Carbon-Carbon Bond Lengths for Organometallic Clusters and Surface Species: Evidence for sp and sp^2 Hybridization of the Apical Carbon for $YCCo_3(CO)_9$

$C_{sp}-C_{sp}$		$C_{sp^2}-C_{sp^2}$	
$HC{\equiv}C{-}{-}C{\equiv}CH$[28]	1.37 Å	$H_2C{=}HC{-}{-}CH{=}CH_2$[28]	1.48 Å
$(CO)_9Co_3C{-}{-}CCo_3(CO)_9$[29]	1.37	$(\pi\text{-}C_6H_3Me_3)(CO)_6Co_3C{-}{-}C_6H_5$[36]	1.48
$(CO)_9Co_3C{-}{-}C{\equiv}C\text{-}CCo_3(CO)_3$ [30]	1.37	$(\pi\text{-}C_8H_8)(CO)_6Co_3C$ $-{-}C_6H_5$[36]	1.47
$(CO)_9Co_3C{-}{-}C{\equiv}C\text{-}[C_3Co_5(CO)_{15}]$[31]	1.36		

$C_{sp^2}-C_{sp^3}$		$C_{sp}-C_{sp^3}$	
$H_2C{=}CH{-}{-}CH_3$[28]	1.51 Å	$HC{\equiv}C{-}{-}CH_3$[28]	1.46 Å
$(CO)_9Co_3C{-}{-}CH_3$[32]	1.53	$Rh(111)\text{-}(2x2)C{-}{-}CH_3$ probably	1.45
$(CO)_9H_3Ru_3C{-}{-}CH_3$[33]	1.51		
$(CO)_9H_3Os_3C{-}{-}CH_3$[34]	1.51		
$[P(C_6H_5)_3](CO)_9Co_3C{-}{-}CH_3$[35]	1.50		

Table IV

Comparison of Apical Carbon Covalent Radii for Alkylidyne Clusters and Ethylidyne on Rh(111). (c = carbon-carbon distance, m = metal-carbon distance, r_M = measured metallic radius, r_C = carbon covalent radius)

		c(Å)	m(Å)	r_M(Å)	r_C(Å)=m-r_M
I.	M_3CCH_3, M_3C-C , or M_3C-O-				
1)	$Co_3(CO)_9CCH_3$[32]	1.53(3)	1.90(2)	1.24	0.66
2)	$H_3Ru_3(CO)_9CCH_3$[33]	1.51(2)	2.08(1)	1.42	0.66
3)	$H_3Os_3(CO)_9CCH_3$[34]	1.51	2.08	1.42	0.66
4)	$(CO)_9Co_3COBH_2N(C_2H_5)_3$[38]	--	1.92(1)	1.25	0.67
5)	$(CO)_9Co_3COBCl_2N(C_2H_5)_3$[39]	--	1.89(2)	1.24	0.67
6)	$(CO)_8[P(C_6H_5)_3]Co_3CCH_3$[40]	1.50(2)	1.91(2)	1.25	0.66
7)	$(CO)_6(\pi\text{-}C_6H_5Me_3)Co_3CPh$[36]	1.48(2)	1.89(2)	1.23	0.66
8)	$(CO)_6(\pi\text{-}C_8H_8)Co_3CPh$[36]	1.48(2)	1.89(2)	1.23	0.66
II.	Rh(111) - (2x2) - C_2H_3				
9)	average	1.45	2.03	1.34	0.69
10)	θ = 0°	1.41	2.03	1.34	0.69
11)	11°	1.44	2.03	1.34	0.69
12)	21°	1.49	2.01	1.34	0.67
13)	31°	1.46	2.03	1.34	0.69
III. 14)	Co_3C-CCo_3[29]	1.37(1)	1.96(1)	1.23	0.73

Table V

Complementary Electronic Evidence for sp- or sp^2-rehybridization and hyperconjugation in $Co_3(CO)_3CCH_3$

Technique	Result	Implication
1) H^1 NMR[29]	δ_H=6.5 ppm for $Co_3(CO)_9CCH_3$--deshielded to C_2H_6 (δ_H=9.1 ppm)--midway between C_2H_4 (δ_H=8.2 ppm) and C_2H_2 (δ_H=4.7)	C-H bond weakening; hyperconjugation
2) H^1 NMR[41]	$\Delta\delta_{H^*}$=0.6 ppm for $Co_3(CO)_9CCH^*_2$ and $Co_3(CO)_9CCH^*_2OH$--$\Delta\delta_{H^*}$ = 8.5 ppm for $Me_2CH^*_2$ and Me_2CH^*OH	positive charge on cluster carbonium ion very delocalized
3) ^{13}C NMR[41]	$\Delta\delta_{C^*}$=13.5 ppm for $Co_3(CO)_9CC^*H_2$ and $Co_3(CO)_9CC^*H_2OH$--$\Delta\delta_{C^*}$ = 255.3 ppm for $Me_2C^*H_2$ and $Me_2C^*H_2OH$--$\Delta\delta_{C^*}$=26.2 ppm for $(C_6H_6)Fe(C_6H_5C^*H_2OH)$ and $(C_6H_6)Fe(C_6H_5C^*H_2)$	positive charge on cluster carbonium ion very delocalized
4) ^{13}C NMR[41]	δ_{C^*} = 258.4 ppm for $Co_3(CO)_9CCO_2Et$—only close to carbyne complexes $RC^*{\equiv}M(CO)_4X$	sp- or sp^2-hybridization of apical carbon
5) ^{59}Co Nuclear Quadrupole Resonance[42]	electron donation or withdrawl from R to CO_3 group in $Co_3(CO)_9CR$ occurs via π-resonance expected for sp- or sp_2-hybridized apical carbon	sp- or sp^2-hybridization of apical carbon

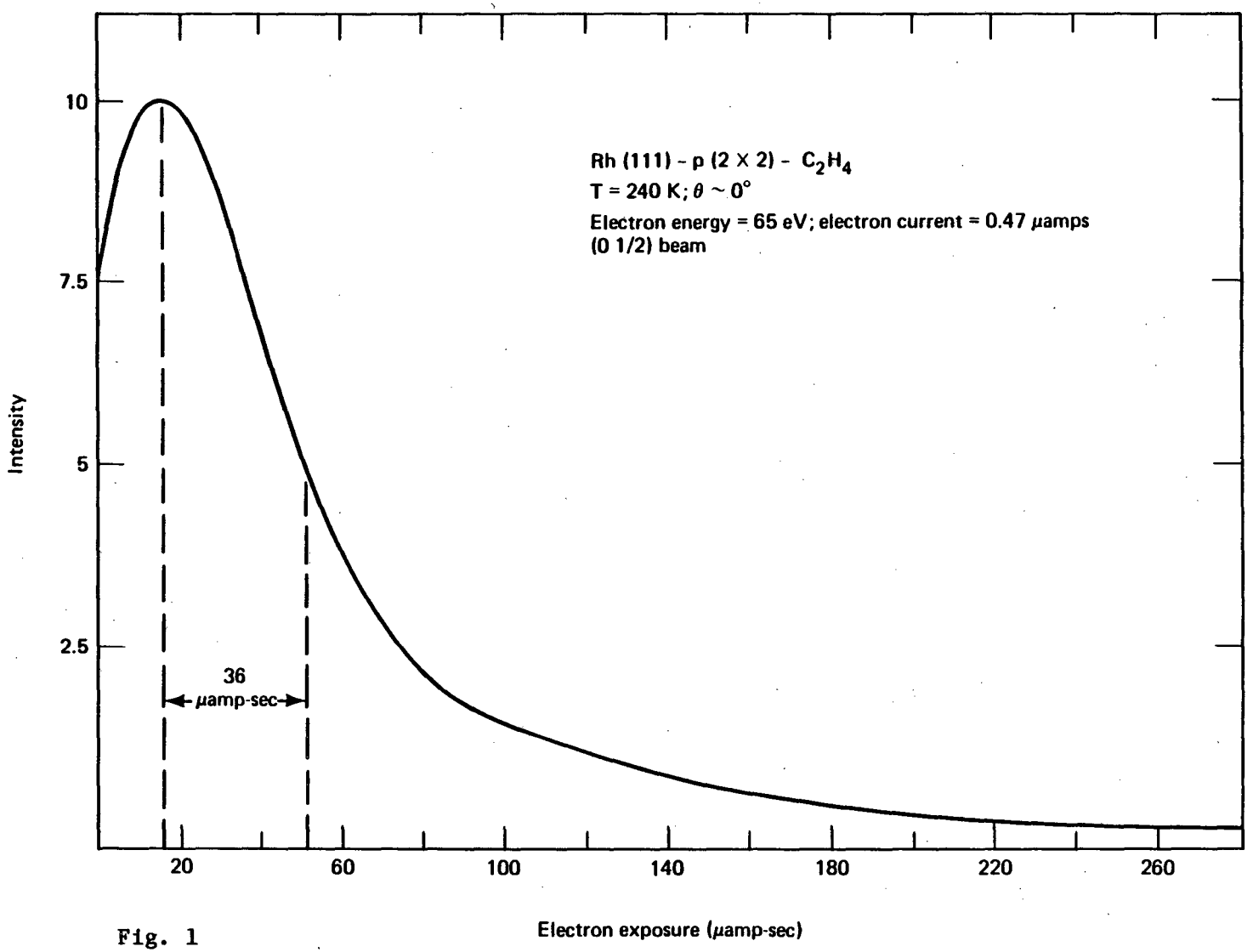

Fig. 1

XBL 818-1092

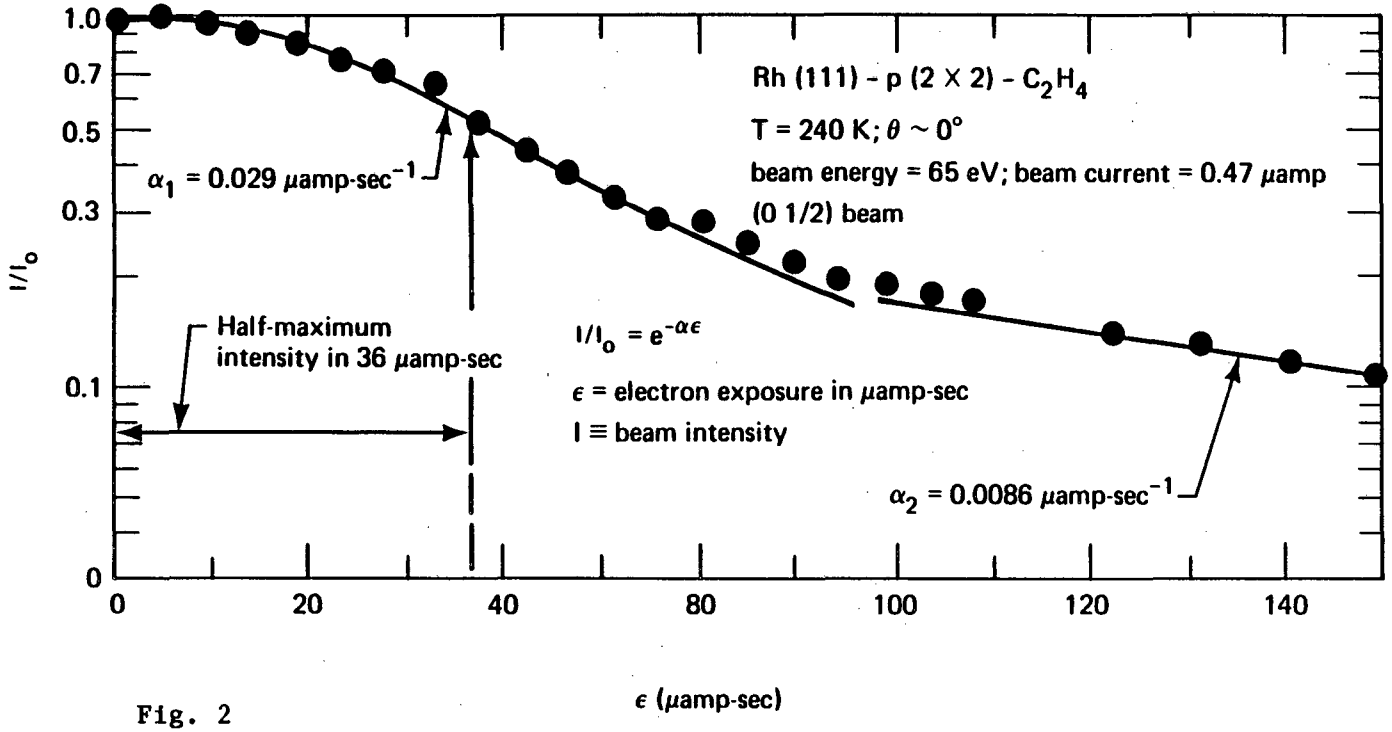

Fig. 2

XBL 818-11195

XBB 788-10161

Fig. 3

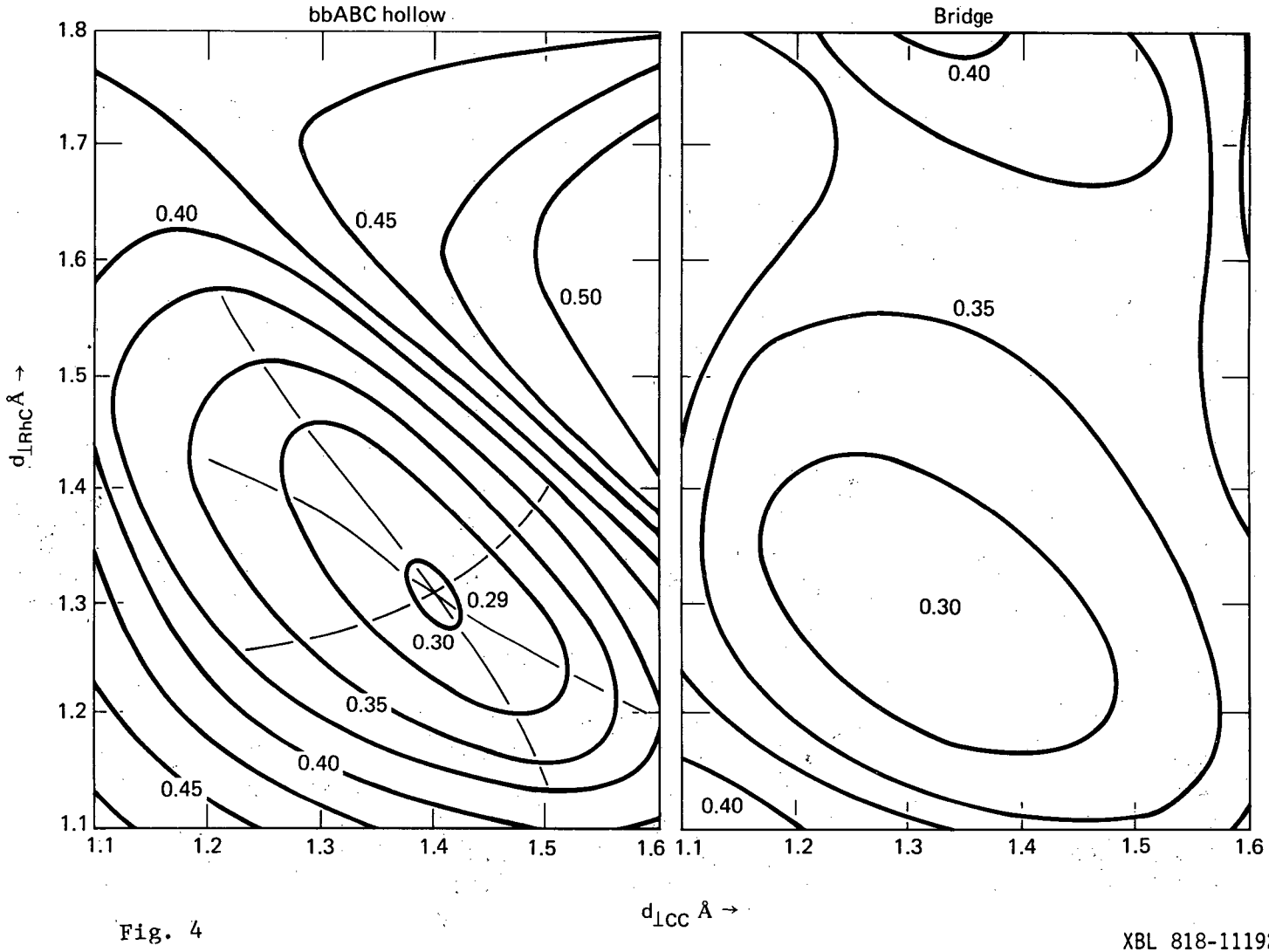

Fig. 4

XBL 818-11192

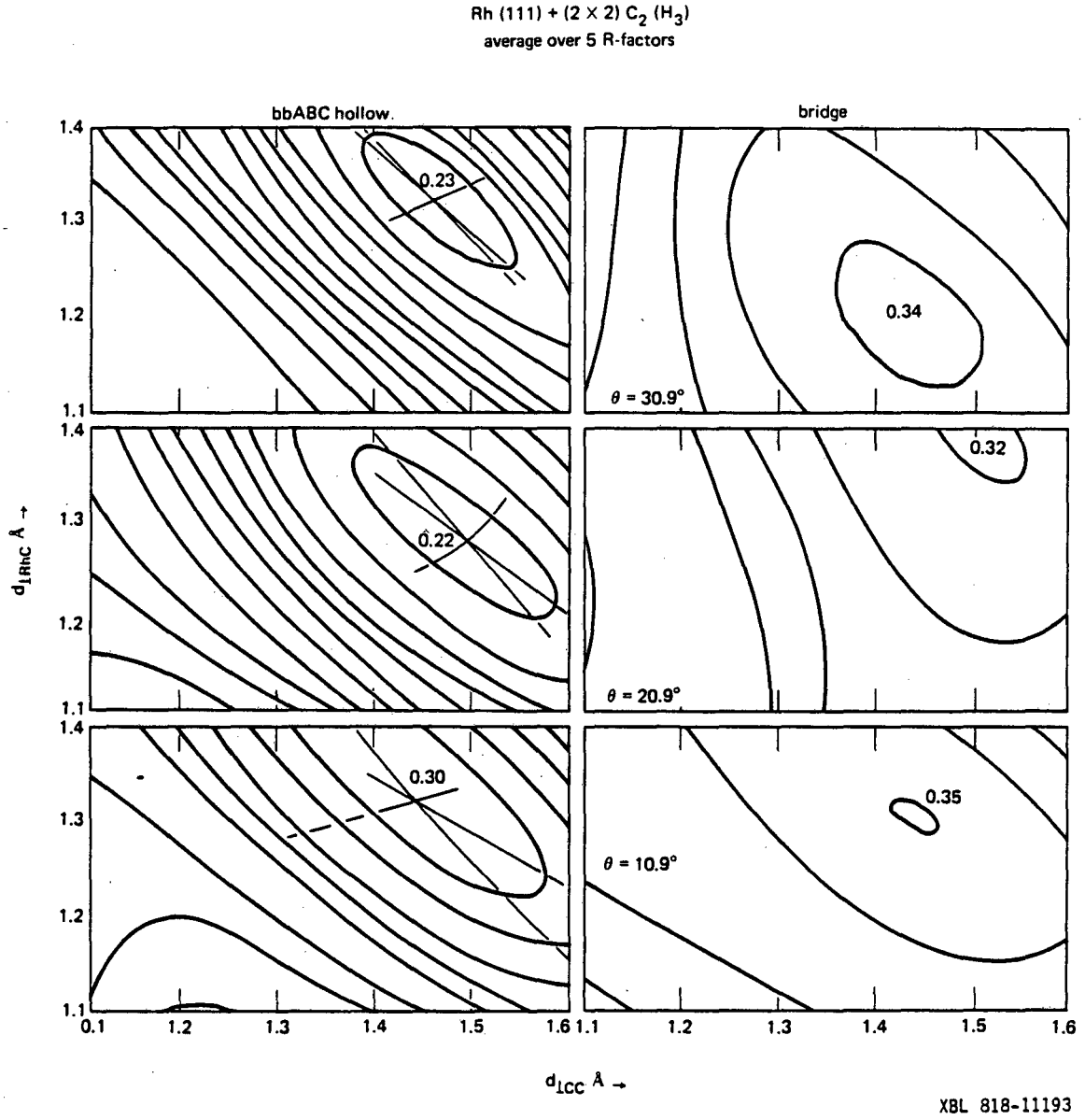
Rh (111) + (2 X 2) C_2 (H_3)
average over 5 R-factors
bbABC hollow
bridge
0.23
0.34
θ = 30.9°
0.22
0.32
θ = 20.9°
0.30
0.35
θ = 10.9°
d_{1RhC} Å →
d_{1CC} Å →
1.4
1.3
1.2
1.1
0.1
1.2
1.3
1.4
1.5
1.6
XBL 818-11193

Fig. 5

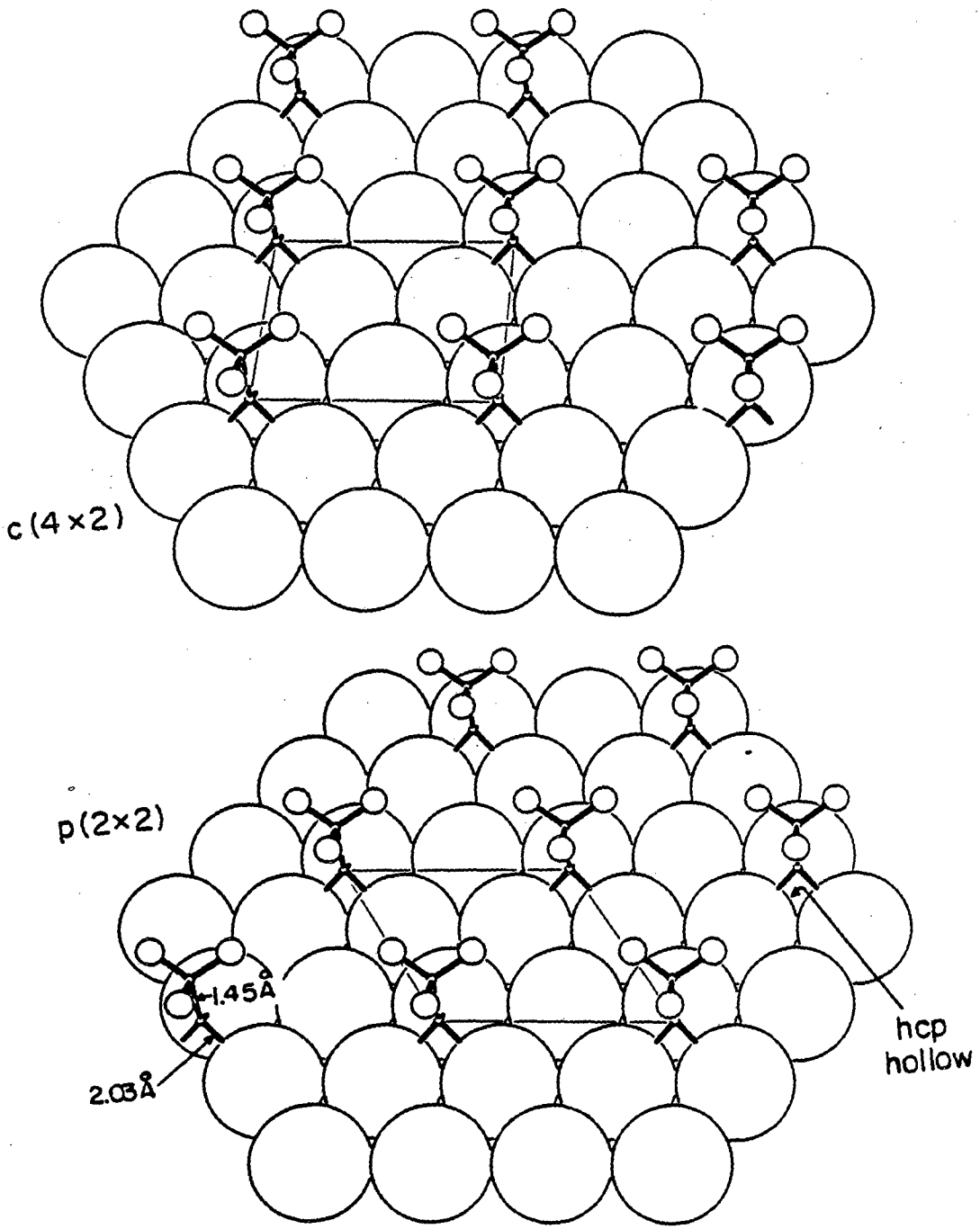

fcc (111) + C_2H_3 (ethylidyne)

XBL813-5407A

Fig. 6

TECHNICAL INFORMATION DEPARTMENT
LAWRENCE BERKELEY LABORATORY
UNIVERSITY OF CALIFORNIA
BERKELEY, CALIFORNIA 94720